Journal of Computational Physics 228 (2009) 921–932

Contents lists available at ScienceDirect

Journal of Computational Physics

journal homepage: www.elsevier.com/locate/jcp

Multilevel fast multipole algorithm for elastic wave scattering by large three-dimensional objects

Mei Song Tong, Weng Cho Chew *,[1]

Center for Computational Electromagnetics and Electromagnetics Laboratory, Department of Electrical and Computer Engineering, University of Illinois at Urbana-Champaign, Urbana, IL 61801, USA

ARTICLE INFO

Article history:
Received 27 February 2008
Received in revised form 18 July 2008
Accepted 6 October 2008
Available online 15 October 2008

Keywords:
Multilevel fast multipole algorithm
Elastic wave scattering
Boundary integral equation

ABSTRACT

Multilevel fast multipole algorithm (MLFMA) is developed for solving elastic wave scattering by large three-dimensional (3D) objects. Since the governing set of boundary integral equations (BIE) for the problem includes both compressional and shear waves with different wave numbers in one medium, the double-tree structure for each medium is used in the MLFMA implementation. When both the object and surrounding media are elastic, four wave numbers in total and thus four FMA trees are involved. We employ Nyström method to discretize the BIE and generate the corresponding matrix equation. The MLFMA is used to accelerate the solution process by reducing the complexity of matrix–vector product from $O(N^2)$ to $O(N \log N)$ in iterative solvers. The multiple-tree structure differs from the single-tree frame in electromagnetics (EM) and acoustics, and greatly complicates the MLFMA implementation due to the different definitions for well-separated groups in different FMA trees. Our Nyström method has made use of the cancellation of leading terms in the series expansion of integral kernels to handle hyper singularities in near terms. This feature is kept in the MLFMA by seeking the common near patches in different FMA trees and treating the involved near terms synergistically. Due to the high cost of the multiple-tree structure, our numerical examples show that we can only solve the elastic wave scattering problems with 0.3–0.4 millions of unknowns on our Dell Precision 690 workstation using one core.

1. Introduction

The fast multipole method (FMM), also known as fast multipole algorithm (FMA) in electromagnetics (EM), was first proposed by Rokhlin [1] as an accelerator for integral equation solvers. This method has been greatly developed and widely used in various areas of science and engineering, such as astrophysics, molecular dynamics and electrical engineering [2–7,11]. The distinct characteristic of the method is the rapid evaluation of matrix–vector multiply in an iterative solver of matrix equation by decomposing the integral kernels into radiation patterns, translators and receiving patterns. This decomposition removes the necessity of explicit storage of matrix elements except for those related to near interaction, leading to a matrix-free scheme. Also, for dynamic problems, the development of multilevel scheme for FMA (resulting in multilevel FMA or MLFMA), with the use of the diagonalization in the translator and the interpolation or anterpolation in radiation and receiving patterns, reduces the complexity of solution process from $O(N^2)$ to $O(N \log N)$ in iterative solvers, where N is the number

* Corresponding author. Tel.: +1 217 333 7309; fax: +1 217 244 7345.
E-mail addresses: w-chew@uiuc.edu, wcchew@hku.edu (W.C. Chew).
URL: http://www.ccem.uiuc.edu (W.C. Chew).
[1] On LOA to serve at The University of Hong Kong.

0021-9991/$ - see front matter © 2008 Published by Elsevier Inc.
doi:10.1016/j.jcp.2008.10.003

of unknowns in the matrix equation. When N is very large, there exists a big difference between these two cost scales and the latter makes possible the solutions of very large problems with millions of unknowns on ordinary workstations. The influence of the method is so profound in science and engineering that it has been recognized as one of top 10 algorithms along with Dantzig's simplex method, Krylov subspace iteration, fast Fourier transform, etc., in 20th century [12].

As pointed out in a review article for FMM [13], the most impressive development for the method is in electrical engineering where workers use the method to solve very large problems by extending the method to MLFMA [5–7]. A typical application for this method is to calculate electromagnetic scattering by aircrafts in which millions of unknowns are involved in the discretization of integral equations [14]. The solutions for the problems with 10–20 million unknowns have been reported several years ago [15–17], and most recently, the problem with more than 85 millions of unknowns has also been solved in a parallel scheme [18,19].

Compared to the rapid development of FMA in electrical engineering, the BIE community in applied mechanics seems to remain less active with respect to FMM [13], even in recent years. Particularly, very few publications can be found for elastodynamic applications of the method. In those papers [20–25] mentioned by the review article [13], the first three only applied FMA to solve 2D problems for elastic wave scattering by rough interface or by many cavities and cracks or in the time domain. The other publications dealt with 3D problems but the maximum number of unknowns was $N = 24,576$ [25]. There is no significant advance in recent years, i.e. after the review paper in terms of our literature search. Some recent works also mainly focused on 2D case, elastostatic case or the time-domain approach for 3D problems [26–29]. We intend to enhance the application of FMA in elastodynamics by presenting this work in which the MLFMA is developed for solving elastic wave scattering by large 3D objects in the frequency domain.

Unlike the acoustic wave and electromagnetic (EM) wave BIE's in which only one wave exists, the elastic wave BIE includes multiple waves and more complicated kernels. Hence the implementation of the FMA is quite different. Since FMA is based on the addition theorem for the Green's function and the kernel for one medium involves two different scalar Green's functions: one for the compressional wave and the other for the shear wave, we need to create two different FMA trees for one medium. If Nyström method is used as a matrix equation generator underlying the FMA and we wisely formulate the radiation and receiving patterns, there will be nine radiation and receiving patterns and nine matrix–vector multiplications are needed in each iteration.

Since multiple trees are used, the difference of wave numbers in different trees leads to the different definitions for well-separated groups by which the near terms and far terms are defined. The far terms are handled with the MLFMA but the near terms are still generated with the based Nyström method. In our original Nyström method implementation without MLFMA acceleration [30], we evaluate the near terms by combining the two scalar Green's functions in the kernels, viz. the compressional wave Green's function and shear wave Green's function. This combination will cancel the hyper singularity in the leading terms of the series expansion of the scalar Green's functions, resulting in weakly singular $1/R$ and $1/R^2$ kernels, where R is the distance between a field point and a source. However, the multiple-tree structure in MLFMA will destroy the combination and require the evaluation of both near terms and far terms tree by tree. Fortunately, we can re-combine those near terms from different trees by searching the common near patches and evaluate them using the scheme in the original Nyström method with appropriate reformulation.

We have implemented the proposed MLFMA as demonstrated in numerical examples. Due to the high cost of the multiple-tree structure and the complexity of integral kernels, we can only solve the elastic wave scattering problems with 0.3–0.4 millions of unknowns currently on our Dell Precision 690 workstation. This machine has two dual-core 3.0 GHz processors and 16 GB RAM, but we only use one core in the series implementation. Hence, the memory usage is intentionally limited to within 12 GB.

2. MLFMA

MLFMA has been introduced in details by many publications, such as [8–11], and is not repeated here. We only present several key formulas to facilitate the description of implementing this algorithm for solving elastic wave scattering problems. In the iterative solution of matrix equation, the bottleneck is the matrix–vector multiply which requires $\mathcal{O}(N^2)$ operations in each iteration. MLFMA changes the computing strategy of the matrix–vector product for far-interaction terms by factorizing the Green's function with diagonal factors, applying interpolation and anterpolation between levels, using an inverted tree structure in the calculation. It includes three stages, i.e. aggregation, translation and disaggregation for calculating the far interaction between the grouped source points and field points. Consider a typical matrix equation

$$\sum_{i=1}^{N} A_{ji} a_i = b_j, \quad j = 1, \ldots, N \tag{1}$$

where N is the total number of unknowns after discretizing an integral equation, b_j is the known excitation in a wave equation, a_i is the unknown coefficient to be solved, and A_{ji} is the element of the matrix. In wave physics, the matrix element A_{ji} is related to the scalar Green's function which can be expanded as [8]

$$\frac{e^{ikr_{ji}}}{r_{ji}} = \int d^2\hat{k} e^{i\mathbf{k}\cdot(\mathbf{r}_{jm} - \mathbf{r}_{im'})} \alpha_{mm'}(\mathbf{k}, \mathbf{r}_{mm'}) \tag{2}$$

where

$$\alpha_{mm'}(\mathbf{k},\mathbf{r}_{mm'}) = \frac{ik}{4\pi}\sum_{l=0}^{L} i^l(2l+1)h_l^{(1)}(kr_{mm'})P_l(\hat{r}_{mm'}\cdot\hat{k}) \tag{3}$$

is the translator. Here, we have chosen $\mathbf{r}_m$ and $\mathbf{r}_{m'}$ as the centers of the mth and m'th groups in which the field point $\mathbf{r}_j$ and source point $\mathbf{r}_i$ reside, respectively. Usually the integral kernels in wave integral equations will include the gradient operation on the scalar Green's function. The expansion for integral kernels can be obtained by simply replacing the gradient ∇ in space domain with multiplication of $i\mathbf{k}$ in the $\hat{k}$-domain in Eq. (2). Thus the matrix element in (1) can be written as

$$A_{ji} = \int d^2\hat{k} V_{fmj}(\hat{k})\cdot\alpha_{mm'}(\mathbf{k},\mathbf{r}_{mm'})V_{sm'i}(\hat{k}) \tag{4}$$

where

$$\begin{aligned} V_{fmj}(\hat{k}) &= \int_{\Delta S_j} dS e^{i\mathbf{k}\cdot\mathbf{r}_{jm}} \\ V_{sm'i}(\hat{k}) &= \int_{\Delta S_i} dS e^{-i\mathbf{k}\cdot\mathbf{r}_{im'}} f(\hat{k}) \end{aligned} \tag{5}$$

are the receiving pattern (aggregation stage) and radiation pattern (disaggregation stage), respectively. In the above, $f(\hat{k})$ denotes the $\hat{k}$-domain representation for the operation acting on the scalar Green's function in the integral kernels.

In the multilevel implementation, the outgoing wave expansions in the radiation pattern are calculated at the finest level and then the expansions for higher levels are obtained by interpolation. Similarly, the anterpolation or transpose interpolation is used to get the incoming wave expansion at a lower level from that at its parent level in the receiving pattern. The interpolation or anterpolation is the key technique for reducing cost and computational complexity in MLFMA.

3. MLFMA formulas for elastic wave scattering

Consider the typical elastic wave scattering by a 3D elastic object embedded in a homogeneous elastic medium, as shown in Fig. 1. The elasticity of a medium is characterized by (ρ,λ,μ), where ρ is the mass density, λ is the bulk modulus, and μ is the shear modulus. The subscript 1 denotes the surrounding medium and 2 denotes the object. The governing BIE for the problem can be found that [31,32]

$$\begin{aligned} &\frac{1}{2}\mathbf{u}(\mathbf{x}) + \int_S \left[\overline{\mathbf{T}}_1^T(\mathbf{x},\mathbf{x}')\cdot\mathbf{u}(\mathbf{x}') - \overline{\mathbf{G}}_1^T(\mathbf{x},\mathbf{x}')\cdot\mathbf{t}(\mathbf{x}')\right]dS' = \mathbf{u}^I(\mathbf{x}), \quad \mathbf{x}\in S \\ &\frac{1}{2}\mathbf{u}(\mathbf{x}) + \int_S \left[\overline{\mathbf{G}}_2^T(\mathbf{x},\mathbf{x}')\cdot\mathbf{t}(\mathbf{x}') - \overline{\mathbf{T}}_2^T(\mathbf{x},\mathbf{x}')\cdot\mathbf{u}(\mathbf{x}')\right]dS' = 0, \quad \mathbf{x}\in S \end{aligned} \tag{6}$$

where $\mathbf{u}$ and $\mathbf{t}$, the unknowns to be solved, are the total displacement and traction vectors at the surface S of the object, $\overline{\mathbf{G}}$ is the tensor Green's function given by

$$\overline{\mathbf{G}} = \frac{1}{\mu}\left(\overline{\mathbf{I}} + \frac{\nabla\nabla}{k_s^2}\right)g_s(\mathbf{x},\mathbf{x}') - \frac{1}{\gamma}\frac{\nabla\nabla}{k_c^2}g_c(\mathbf{x},\mathbf{x}') \tag{7}$$

and $\overline{\mathbf{T}} = \hat{n}'\cdot\overline{\overline{\Sigma}}(\mathbf{x},\mathbf{x}')$ where $\overline{\overline{\Sigma}}(\mathbf{x},\mathbf{x}') = \lambda\overline{\mathbf{I}}\nabla\cdot\overline{\mathbf{G}} + \mu(\nabla\overline{\mathbf{G}} + \overline{\mathbf{G}}\nabla)$ is a third-rank Green's tensor. $\overline{\mathbf{G}}$ and $\overline{\mathbf{T}}$ are also known as the Stokes' displacement and traction tensors, respectively, and the superscript T on them denotes the transpose. In (7), $g_s = e^{ik_s r}/(4\pi r)$ and $g_c = e^{ik_c r}/(4\pi r)$ are the scalar Green's functions in free space, and $r = |\mathbf{x}-\mathbf{x}'|$ is the distance between a field point $\mathbf{x}$ (without a prime) and a source point $\mathbf{x}'$ (with a prime). The subscript s denotes the shear wave and c denotes

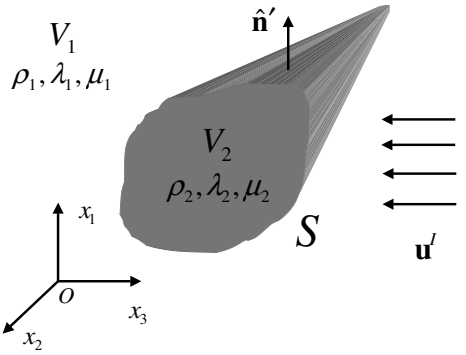

Fig. 1. Elastic wave scattering by a 3D elastic object embedded in an elastic medium.

the compressional wave. The corresponding wave numbers are given by $k_s^2 = \omega^2\rho/\mu$ and $k_c^2 = \omega^2\rho/\gamma$ with $\gamma = \lambda + 2\mu$, and ω is the angular frequency here. Also, the superscript I in (6) denotes an incident wave, the hat on a variable indicates a unit vector, the boldface of a variable implies a vector, single bar over a vector denotes a dyad, double bars over a vector denote a third-rank tensor, and $\bar{\mathbf{I}}$ stands for the identity dyad in (7). If the object is a rigid inclusion or traction-free cavity, the above equations can be simplified and the individual MLFMA formula can be developed for each case.

Note that the multiple trees are needed in the implementation because two waves with different wave numbers exist in each medium. The shear wave has a wave number k_s and the compressional wave has a wave number k_c. The ratio of these two wave numbers will be

$$\frac{k_s}{k_c} = \sqrt{\frac{\gamma}{\mu}} = \sqrt{\frac{\lambda}{\mu} + 2} \tag{8}$$

Since both λ and μ are positive, the above ratio will be greater than $\sqrt{2}$. If the object is elastic, then there are also two wave numbers inside the object which are different from the two wave numbers in the surrounding medium.

Due to the use of multi-tree structure, the computational costs are quite different from those in EM problems. For elastic objects, we have four FMA trees and each tree has an independent aggregation–translation–disaggregation process. Therefore, compared with the single-tree EM problems, the costs will be at least four times. Also, there are nine radiation and receiving patterns in total for each medium (two trees). This is because the unknown vectors in the elastic BIE are three-dimensional (three components) over the boundary (surface) and we use Nyström method to solve it. The unknown vectors (electric and magnetic currents) in EM surface integral equation (SIE) are two-dimensional, namely, they are surface vectors. If we use the solving process for EM SIE to solve the elastic BIE, namely, use the method of moments (MoM) with Rao-Wilton-Glisson (RWG) basis for expanding the surface component and pulse basis for expanding the normal component of unknown vectors in the elastic BIE, the number of patterns will be four. The other contribution to the difference of the "CONSTANT" in the computational complexity expression comes from the big difference in formulations between these two types of problems. From Eqs. (26) and (27) in Section 4, we can see that the kernels in elastic BIE are much complex than those in EM SIE, so the implementation costs are also much higher.

3.1. Scattering by a rigid object

If the object is rigid, the unknown displacement vector on the surface vanishes and the above BIE becomes

$$\int_S \bar{\mathbf{G}}_1^T(\mathbf{x},\mathbf{x}') \cdot \mathbf{t}(\mathbf{x}')dS' = -\mathbf{u}^I(\mathbf{x}), \quad \mathbf{x} \in S. \tag{9}$$

From (7), we can see that the above kernel $\bar{\mathbf{G}}$ includes two parts. One is related to the shear wave Green's function g_s and the other, to the compressional wave Green's function g_c. We have to create an individual FMA tree for each of the two Green's functions so that the far-interaction terms between the ith source point and jth field point can be calculated by

$$A_{ji}^w = \int d^2\hat{k}_w V_{fmj}^w(\hat{k}_w) \cdot \alpha_{mm'}^w(\mathbf{k}_w, \mathbf{r}_{mm'}) V_{sm'i}^w(\hat{k}_w), \quad w = s \text{ or } c \tag{10}$$

where $V_{sm'i}^w$ and V_{fmj}^w are radiation pattern and receiving pattern, respectively, and $\alpha_{mm'}^w$ is the translator. They are defined for the shear wave when $w = s$ and the compressional wave when $w = c$, respectively. From the above kernel and the identity for the scalar Green's function (2), we can find the corresponding receiving pattern and radiation pattern as follows:

$$\begin{aligned}
V_{fmj}^s(\hat{k}_s) &= \frac{e^{i\mathbf{k}_s\cdot\mathbf{r}_{jm}}}{4\pi\mu} \\
V_{fmj}^c(\hat{k}_c) &= \frac{e^{i\mathbf{k}_c\cdot\mathbf{r}_{jm}}}{4\pi\gamma} \\
\bar{\mathbf{V}}_{sm'i}^s(\hat{k}_s) &= \int_{\Delta S_i} dS' \bar{\mathbf{E}}_s e^{-i\mathbf{k}_s\cdot\mathbf{r}_{im'}} \\
\bar{\mathbf{V}}_{sm'i}^c(\hat{k}_c) &= \int_{\Delta S_i} dS' \bar{\mathbf{E}}_c e^{-i\mathbf{k}_c\cdot\mathbf{r}_{im'}}
\end{aligned} \tag{11}$$

where

$$\begin{aligned}
\bar{\mathbf{E}}_s &= \sum_{i=1}^{3}\sum_{j=1}^{3} E_{ij}^s \hat{x}_i\hat{x}_j \\
\bar{\mathbf{E}}_c &= \sum_{i=1}^{3}\sum_{j=1}^{3} E_{ij}^c \hat{x}_i\hat{x}_j
\end{aligned} \tag{12}$$

and

$$\begin{aligned}
E_{ij}^s &= \delta_{ij} - k_i^s k_j^s \\
E_{ij}^c &= k_i^c k_j^c
\end{aligned} \tag{13}$$

In the above, we have used the indicial notation in the Cartesian coordinate system and defined $\mathbf{k}_w = k_w \hat{k}_w$ with $\hat{k}_w = k_1^w \hat{x}_1 + k_2^w \hat{x}_2 + k_3^w \hat{x}_3$ ($w = s$ or c). Also, ΔS_i represents a small triangle patch in the discretization of the object surface S and δ_{ij} is the Kronecker delta.

3.2. Scattering by a traction-free cavity

If the object is a traction-free cavity such as a bubble in elastic material, the unknown traction vector at the surface vanishes and the BIE is reduced to

$$\frac{1}{2}\mathbf{u}(\mathbf{x}) + \int_S \overline{\mathbf{T}}_1^T(\mathbf{x},\mathbf{x}') \cdot \mathbf{u}(\mathbf{x}') dS' = \mathbf{u}^I(\mathbf{x}), \quad \mathbf{x} \in S \tag{14}$$

The integral kernel can be written into two parts, i.e.

$$\overline{\mathbf{T}} = \hat{n}' \cdot \overline{\overline{\Sigma}}(\mathbf{x},\mathbf{x}') = \lambda \hat{n}' \nabla \cdot \overline{\mathbf{G}} + \mu \hat{n}' \cdot (\nabla \overline{\mathbf{G}} + \overline{\mathbf{G}} \nabla) = \overline{\mathbf{A}} + \overline{\mathbf{B}} \tag{15}$$

where

$$\begin{aligned} \overline{\mathbf{A}} &= \lambda \hat{n}' \nabla \cdot \overline{\mathbf{G}} = \frac{\lambda}{\gamma} \hat{n}' \nabla g_c \\ \overline{\mathbf{B}} &= \mu \hat{n}' \cdot (\nabla \overline{\mathbf{G}} + \overline{\mathbf{G}} \nabla) \end{aligned} \tag{16}$$

The first part is only related to the compressional wave and its expansion in $\hat{k}$ domain can be found as

$$\overline{\mathbf{A}} = \int d^2 \hat{k}_c e^{i\mathbf{k}_c \cdot \mathbf{r}_{jm}} \cdot \alpha_{mm'}(\mathbf{k}_c, \mathbf{r}_{mm'}) \overline{\mathbf{Q}}_c e^{-i\mathbf{k}_c \cdot \mathbf{r}_{im'}} \tag{17}$$

where

$$\overline{\mathbf{Q}}_c = c_3 \sum_{i=1}^{3} \sum_{j=1}^{3} q_{ij}^c \hat{x}_i \hat{x}_j \tag{18}$$

with $c_3 = i\lambda k_c/\gamma$ and $q_{ij}^c = n_i' k_j^c$. Here n_i' is a component of the unit normal vector on the object surface $\hat{n}'$, i.e., $\hat{n}' = n_1' \hat{x}_1 + n_2' \hat{x}_2 + n_3' \hat{x}_3$.

The second part includes both shear wave and compressional wave and we can separate these two waves in $\hat{k}$ domain, i.e.

$$\overline{\mathbf{B}} = \int d^2 \hat{k}_s e^{i\mathbf{k}_s \cdot \mathbf{r}_{jm}} \cdot \alpha_{mm'}(\mathbf{k}_s, \mathbf{r}_{mm'}) \overline{\mathbf{P}}_s e^{-i\mathbf{k}_s \cdot \mathbf{r}_{im'}} - \int d^2 \hat{k}_c e^{i\mathbf{k}_c \cdot \mathbf{r}_{jm}} \cdot \alpha_{mm'}(\mathbf{k}_c, \mathbf{r}_{mm'}) \overline{\mathbf{P}}_c e^{-i\mathbf{k}_c \cdot \mathbf{r}_{im'}} \tag{19}$$

where

$$\begin{aligned} \overline{\mathbf{P}}_s &= c_1 \sum_{i=1}^{3} \sum_{j=1}^{3} p_{ij}^s \hat{x}_i \hat{x}_j \\ \overline{\mathbf{P}}_c &= c_2 \sum_{i=1}^{3} \sum_{j=1}^{3} p_{ij}^c \hat{x}_i \hat{x}_j \end{aligned} \tag{20}$$

and

$$\begin{aligned} c_1 &= -\frac{2i\mu k_s^3}{4\pi\omega^2\rho} \\ c_2 &= -\frac{2i\mu k_c^3}{4\pi\omega^2\rho} \\ p_{ij}^s &= k_i^s k_j^s (n_1' k_1^s + n_2' k_2^s + n_3' k_3^s) \\ p_{ij}^c &= k_i^c k_j^c (n_1' k_1^c + n_2' k_2^c + n_3' k_3^c) \end{aligned} \tag{21}$$

After combining these two parts together, the corresponding receiving pattern and radiation pattern for the kernel can be written as

$$\begin{aligned} V_{fmj}^s(\hat{k}_s) &= e^{i\mathbf{k}_s \cdot \mathbf{r}_{jm}} \\ \overline{\mathbf{V}}_{sm'i}^s(\hat{k}_s) &= \sum_{i=1}^{3} \sum_{j=1}^{3} (c_1 p_{ij}^s + c_4 q_{ij}^s) \int_{\Delta S_i} dS' e^{-i\mathbf{k}_s \cdot \mathbf{r}_{im'}} \\ V_{fmj}^c(\hat{k}_c) &= e^{i\mathbf{k}_c \cdot \mathbf{r}_{jm}} \\ \overline{\mathbf{V}}_{sm'i}^c(\hat{k}_c) &= \sum_{i=1}^{3} \sum_{j=1}^{3} (c_3 q_{ij}^c - c_2 p_{ij}^c) \int_{\Delta S_i} dS' e^{-i\mathbf{k}_c \cdot \mathbf{r}_{im'}} \end{aligned} \tag{22}$$

where

$$q_{ij}^s = n_i' k_j^s + \delta_{ij}(n_1' k_1^s + n_2' k_2^s + n_3' k_3^s) \tag{23}$$

and $c_4 = c_1/2$. Note that we do not include the identity or constant term $(1/2)$ of the BIE in the receiving pattern or radiation pattern because it belongs to near terms (diagonal terms) which MLFMA will not work on.

3.3. Scattering by an elastic object

If both the object and the surrounding medium are elastic, we have two BIE's corresponding to the waves in the exterior medium and interior medium of the object. In each medium, there are two types of waves, i.e. shear wave and compressional wave, so we have four wave numbers in total and need four FMA trees. In an indicial notation, the BIE's in (6) can be written as

$$\begin{aligned}
&\frac{1}{2}u_i + \int_S \sum_{j=1}^{3}\left[-G_{ij}^{(1)} t_j' + T_{ij}^{(1)} u_j'\right] dS' = u_i^I \\
&\frac{1}{2}u_i + \int_S \sum_{j=1}^{3}\left[G_{ij}^{(2)} t_j' - T_{ij}^{(2)} u_j'\right] dS' = 0 \\
&i = 1,2,3
\end{aligned} \tag{24}$$

or in a matrix form

$$\begin{bmatrix}
-G_{11}^{(1)} & -G_{21}^{(1)} & -G_{31}^{(1)} & T_{11}^{(1)} & T_{21}^{(1)} & T_{31}^{(1)} \\
-G_{12}^{(1)} & -G_{22}^{(1)} & -G_{32}^{(1)} & T_{12}^{(1)} & T_{22}^{(1)} & T_{32}^{(1)} \\
-G_{13}^{(1)} & -G_{23}^{(1)} & -G_{33}^{(1)} & T_{13}^{(1)} & T_{23}^{(1)} & T_{33}^{(1)} \\
G_{11}^{(2)} & G_{21}^{(2)} & G_{31}^{(2)} & -T_{11}^{(2)} & -T_{21}^{(2)} & -T_{31}^{(2)} \\
G_{12}^{(2)} & G_{22}^{(2)} & G_{32}^{(2)} & -T_{12}^{(2)} & -T_{22}^{(2)} & -T_{32}^{(2)} \\
G_{13}^{(2)} & G_{23}^{(2)} & G_{33}^{(2)} & -T_{13}^{(2)} & -T_{23}^{(2)} & -T_{33}^{(2)}
\end{bmatrix}
\begin{bmatrix} t_1' \\ t_2' \\ t_3' \\ u_1' \\ u_2' \\ u_3' \end{bmatrix}
=
\begin{bmatrix} u_1^I \\ u_2^I \\ u_3^I \\ 0 \\ 0 \\ 0 \end{bmatrix}. \tag{25}$$

In the matrix form, we again omit the identity or constant terms (1/2) of the BIE's because MLFMA only acts on far-interaction terms. Each matrix element above includes sub-kernels related to shear wave and compressional wave, respectively. These sub-kernels can be calculated for far interactions by following the MLFMA formulas developed in the previous sections for the rigid object and traction-free cavity.

4. Reformulation of near terms

The near terms in the original Nyström method without MLFMA acceleration are calculated in the integrated form of the kernels [30]. Now we have to separate the compressional wave part from the shear wave part in the kernels because they belong to different FMA trees and reformulate the expressions for common near patches after cancelling the strongest singularities. The kernels in indicial notation can be found that [30]

$$\begin{aligned}
G_{ij} &= (\overline{\mathbf{G}})_{ij} = \frac{c_0}{r^3}\{\delta_{ij}[(k_s r)^2 e^{ik_s r} + D] + C\partial_i r \partial_j r\} \\
T_{ij} &= (\hat{n}' \cdot \overline{\overline{\mathbf{\Sigma}}})_{ij} \\
&= \frac{c_0}{r^4}\left\{\lambda e^{ik_c r}(k_c r)^2 (ik_c r - 1) n_i \partial_j r + \mu e^{ik_s r}(k_s r)^2 (ik_s r - 1)\left(\delta_{ij}\frac{\partial r}{\partial n} + n_i \partial_j r\right) + 2\mu\left[C\left(\delta_{ij}\frac{\partial r}{\partial n} + n_i \partial_j r + n_j \partial_i r\right) + F\partial_i r \partial_j r \frac{\partial r}{\partial n}\right]\right\}
\end{aligned} \tag{26}$$

where $\partial_i r = \partial r/\partial x_i$, $\partial_j r = \partial r/\partial x_j$, and

$$\begin{aligned}
c_0 &= \frac{1}{4\pi\rho\omega^2} \\
C &= \Omega_s e^{ik_s r} - \Omega_c e^{ik_c r} \\
D &= (ik_s r - 1)e^{ik_s r} - (ik_c r - 1)e^{ik_c r} \\
F &= H_c e^{ik_c r} - H_s e^{ik_s r} \\
\Omega_s &= 3 - 3ik_s r - k_s^2 r^2 \\
\Omega_c &= 3 - 3ik_c r - k_c^2 r^2 \\
H_s &= 15 - 15ik_s r - 6k_s^2 r^2 + ik_s^3 r^3 \\
H_c &= 15 - 15ik_c r - 6k_c^2 r^2 + ik_c^3 r^3.
\end{aligned} \tag{27}$$

If we use the series expansion of the scalar Green's function

$$\frac{e^{ikr}}{r} = \sum_{m=0}^{\infty} \frac{(ik)^m r^{m-1}}{m!} \approx \sum_{m=0}^{M} \frac{(ik)^m r^{m-1}}{m!} \tag{28}$$

the leading terms in the kernels, which include the strongest singularities, will be cancelled. Since the expansion is only applied to the near terms with a small r, the series converges very fast. The typical M is chosen as 10 and the accuracy of the series can reach 10^{-8} when $r = 0.1$ and $k = 2\pi$ (unit wavelength).

With the use of the series expansion and the cancellation of the strongest singularities in the kernels, we obtain

$$\begin{aligned} G_{ij} &= c_0 \left\{ \left[\frac{2}{r}(k_s^2 - k_c^2) - i(k_s^3 - k_c^3) \right] \partial_i r \partial_j r + \frac{\delta_{ij}}{r}(k_c^2 - k_s^2 + k_s^2 e^{ik_s r}) + \sum_{m=2}^{M} \frac{i^m r^{m-3}}{m!} \left[(k_s^m \Omega_s - k_c^m \Omega_c) \partial_i r \partial_j r + \delta_{ij} k_s^m (ik_s r - 1) - \delta_{ij} k_c^m (ik_c r - 1) \right] \right\} \\ T_{ij} &= c_0 \left[\lambda k_c^2 n_i \partial_j r A + \mu k_s^2 \left(\delta_{ij} \frac{\partial r}{\partial n} + n_j \partial_i r \right) B + 2\mu \left(\delta_{ij} \frac{\partial r}{\partial n} P + n_i \partial_j r P + n_j \partial_i r P + \frac{\partial r}{\partial n} \partial_i r \partial_j r Q \right) \right] \end{aligned} \tag{29}$$

where

$$\begin{aligned} A &= \frac{(ik_c r - 1)}{r^2} e^{ik_c r} = -\frac{1}{r^2} - k_c^2 + \sum_{m=2}^{M} \frac{(ik_c)^m}{m!} (ik_c r - 1) r^{m-2} \\ B &= \frac{(ik_s r - 1)}{r^2} e^{ik_s r} = -\frac{1}{r^2} - k_s^2 + \sum_{m=2}^{M} \frac{(ik_s)^m}{m!} (ik_s r - 1) r^{m-2} \\ P &= \frac{1}{r^4}(\Omega_s e^{ik_s r} - \Omega_c e^{ik_c r}) = \frac{1}{2r^2}(k_s^2 - k_c^2) + \frac{ir}{6}(k_s^5 - k_c^5) + \sum_{m=2}^{M} \frac{i^m}{m!}(k_s^m \Omega_s - k_c^m \Omega_c) r^{m-4} \\ Q &= \frac{1}{r^4}(H_c e^{ik_c r} - H_s e^{ik_s r}) = \frac{3}{2r^2}(k_c^2 - k_s^2) - \frac{1}{2}(k_c^4 - k_s^4) + \frac{i}{2}(k_c^5 - k_s^5) r + \frac{1}{6}(k_c^6 - k_s^6) r^2 + \sum_{m=4}^{M} \frac{i^m}{m!}(k_s^m \Omega_s - k_c^m \Omega_c) r^{m-4}. \end{aligned} \tag{30}$$

The FMA trees require to calculate the two parts related to two different wave numbers in the kernels individually, so the above two kernels can be rewritten as

$$\begin{aligned} G_{ij} &= G_{ij}^s + G_{ij}^c \\ T_{ij} &= T_{ij}^s + T_{ij}^c \end{aligned} \tag{31}$$

where

$$\begin{aligned} G_{ij}^s &= c_0 \left\{ \left[\frac{k_s^2}{2r} + \frac{rk_s^4}{8} + \frac{ir^2 k_s^5}{24} - \frac{r^3 k_s^6}{24} + \sum_{m=5}^{M} \frac{(ik_s)^m}{m!} \Omega_s r^{m-5} \right] \partial_i r \partial_j r + \delta_{ij} \left[-\frac{k_s^2}{2r} - \frac{ik_s^3}{2} + \frac{k_s^2 e^{ik_s r}}{r} + \sum_{m=3}^{M} \frac{(ik_s)^m}{m!} (ik_s r - 1) r^{m-3} \right] \right\} \\ G_{ij}^c &= c_0 \left\{ \left[-\frac{k_c^2}{2r} - \frac{rk_c^4}{8} - \frac{ir^2 k_c^5}{24} + \frac{r^3 k_c^6}{24} - \sum_{m=5}^{M} \frac{(ik_c)^m}{m!} \Omega_c r^{m-5} \right] \partial_i r \partial_j r + \delta_{ij} \left[\frac{k_c^2}{2r} + \frac{ik_c^3}{2} - \sum_{m=3}^{M} \frac{(ik_c)^m}{m!} (ik_c r - 1) r^{m-3} \right] \right\} \\ T_{ij}^s &= c_0 \left[2\mu \left(\delta_{ij} \frac{\partial r}{\partial n} P_s + n_i \partial_j r P_s + n_j \partial_i r P_s + \frac{\partial r}{\partial n} \partial_i r \partial_j r Q_s \right) + \mu k_s^2 \left(\delta_{ij} \frac{\partial r}{\partial n} + n_j \partial_i r \right) B \right] \\ T_{ij}^c &= c_0 \left[\lambda k_c^2 n_i \partial_j r A + 2\mu \left(\delta_{ij} \frac{\partial r}{\partial n} P_c + n_i \partial_j r P_c + n_j \partial_i r P_c + \frac{\partial r}{\partial n} \partial_i r \partial_j r Q_c \right) \right] \end{aligned} \tag{32}$$

with

$$\begin{aligned} P_w &= \pm \left[\frac{k_w^2}{2r^2} + \frac{irk_w^5}{6} + \sum_{m=2}^{M} \frac{(ik_w)^m}{m!} \Omega_w r^{m-4} \right] \\ Q_w &= \mp \left[\frac{3k_w^2}{2r^2} - \frac{k_w^4}{2} + \frac{irk_w^5}{2} + \frac{r^2 k_w^6}{6} - \sum_{m=4}^{M} \frac{(ik_w)^m}{m!} \Omega_w r^{m-4} \right] \end{aligned} \tag{33}$$

In the above, $w = s$ or c, and the upper sign is taken when $w = s$ whereas the lower sign is taken when $w = c$. We can see that the above kernels only include the weak $1/R$ and $1/R^2$ singularities and they can be easily handled. We have derived closed-form solutions for these singularities and the treatment technique can be found in [30]. The $1/R^2$ singularity is a strong singularity compared with the $1/R$ singularity but it is weak and much easier to handle compared to the $1/R^3$ hypersingularity. After the two parts are evaluated in the two different FMA tree frames, they will be combined together for common near patches.

5. Reduction of number of patterns

We have shown an implementation scheme for MLFMA in Section 3. This scheme is suitable for the boundary element method (BEM) workers in elastodynamics because we fully follow their conventions to formulate. These conventions include

changing the vector BIE into a scalar form with the use of indicial notations in denoting the components of kernels, and using a collocation procedure to form a matrix equation without basis and testing functions involved. Although the implementation looks very simple, it is not efficient. If we introduce a MOM-like procedure in the Nyström method, the efficiency of implementation can be improved by reducing the number of patterns. Consider the BIE in (9)

$$\int_S \overline{\mathbf{G}}(\mathbf{x},\mathbf{x}')\cdot\mathbf{t}(\mathbf{x}')dS' = -\mathbf{u}^I(\mathbf{x}), \quad \mathbf{x}\in S \tag{34}$$

where we have omitted the transpose on $\overline{\mathbf{G}}$ due to its symmetry and the subscript for simplicity. We can decompose the unknown traction vector $\mathbf{t}$ into three orthogonal components, i.e.

$$\mathbf{t}(\mathbf{x}') = \xi(\mathbf{x}')\hat{\xi}(\mathbf{x}') + \eta(\mathbf{x}')\hat{\eta}(\mathbf{x}') + \zeta(\mathbf{x}')\hat{\zeta}(\mathbf{x}') \tag{35}$$

where $(\hat{\xi},\hat{\eta},\hat{\zeta})$ are three orthogonal unit vectors and $[\xi(\mathbf{x}'),\eta(\mathbf{x}'),\zeta(\mathbf{x}')]$ are three unknown components to be solved. We may choose $\hat{\xi}$ and $\hat{\eta}$ as two unit tangential vectors to the object surface at the point $\mathbf{x}'$ and $\hat{\zeta}$ as the outward normal unit vector at the same point. When discretizing the object surface into N small triangle patches ΔS_i $(i=1,2,\ldots,N)$ and applying a quadrature rule to the integral over a patch, we can rewrite the BIE in (34) as

$$\sum_{i=1}^{N}\sum_{j=1}^{Q}\overline{\mathbf{G}}(\mathbf{x},\mathbf{x}'_{ij})\cdot[\xi(\mathbf{x}'_{ij})\hat{\xi}(\mathbf{x}'_{ij}) + \eta(\mathbf{x}'_{ij})\hat{\eta}(\mathbf{x}'_{ij}) + \zeta(\mathbf{x}'_{ij})\hat{\zeta}(\mathbf{x}'_{ij})]w_{ij} = -\mathbf{u}^I(\mathbf{x}), \quad \mathbf{x}\in S \tag{36}$$

where $\mathbf{x}'_{ij}$ represents the jth quadrature point within the ith patch, w_{ij} is the corresponding weight at the same point, and Q is the total number of quadrature points over a patch. Testing the above discretized equation with $\hat{\xi}$, $\hat{\eta}$ and $\hat{\zeta}$ at an observation point $\mathbf{x}_{pq}$ which is the qth quadrature point in the pth patch, we can obtain a matrix equation

$$\begin{aligned}&\sum_{i=1}^{N}\sum_{j=1}^{Q}\{[\hat{\alpha}(\mathbf{x}_{pq})\cdot\overline{\mathbf{G}}(\mathbf{x}_{pq},\mathbf{x}'_{ij})\cdot\hat{\xi}(\mathbf{x}'_{ij})]w_{ij}\xi(\mathbf{x}'_{ij}) + [\hat{\alpha}(\mathbf{x}_{pq})\cdot\overline{\mathbf{G}}(\mathbf{x}_{pq},\mathbf{x}'_{ij})\cdot\hat{\eta}(\mathbf{x}'_{ij})]w_{ij}\eta(\mathbf{x}'_{ij}) + [\hat{\alpha}(\mathbf{x}_{pq})\cdot\overline{\mathbf{G}}(\mathbf{x}_{pq},\mathbf{x}'_{ij})\\ &\cdot\hat{\zeta}(\mathbf{x}'_{ij})]w_{ij}\zeta(\mathbf{x}'_{ij})\}\\ &= -\hat{\alpha}(\mathbf{x}_{pq})\cdot\mathbf{u}^I(\mathbf{x}_{pq}), \quad \mathbf{x}_{pq}\in S.\end{aligned} \tag{37}$$

where $\hat{\alpha}$ represents $\hat{\xi}$, $\hat{\eta}$ or $\hat{\zeta}$, and $p=1,2,\ldots,N$; $q=1,2,\ldots,Q$. We have two scalar Green's functions in the kernel which are related to the shear wave and compressional wave, respectively, and we need to handle them individually. For the shear wave part, we can write the kernel as

$$\overline{\mathbf{G}}_s(\mathbf{x}_{pq},\mathbf{x}'_{ij}) = \frac{1}{\mu}\left(\overline{\mathbf{I}} + \frac{\nabla\nabla}{k_s^2}\right)g_s(\mathbf{x}_{pq},\mathbf{x}'_{ij}) = \int d^2\hat{k}_s e^{i\mathbf{k}_s\cdot(\mathbf{r}_{bm}-\mathbf{r}_{am'})}\alpha_{mm'}(\mathbf{k}_s,\mathbf{r}_{mm'})(\overline{\mathbf{I}}-\hat{k}_s\hat{k}_s) \tag{38}$$

where the subscript $a=ij$ represents a source point and $b=pq$ denotes an observation point. The terms in the square brackets in the matrix equation (37) are then

$$\hat{\alpha}(\mathbf{x}_{pq})\cdot\overline{\mathbf{G}}_s(\mathbf{x}_{pq},\mathbf{x}'_{ij})\cdot\hat{\beta}(\mathbf{x}'_{ij}) = \hat{\alpha}(\mathbf{x}_{pq})\cdot\frac{1}{\mu}\int d^2\hat{k}_s e^{i\mathbf{k}_s\cdot\mathbf{r}_{bm}}\alpha_{mm'}(\mathbf{k}_s,\mathbf{r}_{mm'})\cdot\left[e^{-i\mathbf{k}_s\cdot\mathbf{r}_{am'}}\cdot(\overline{\mathbf{I}}-\hat{k}_s\hat{k}_s)\cdot\hat{\beta}(\mathbf{x}'_{ij})\right]. \tag{39}$$

where $\hat{\beta}$ also represents $\hat{\xi}$, $\hat{\eta}$ or $\hat{\zeta}$. Since $\overline{\mathbf{I}}-\hat{k}_s\hat{k}_s = \hat{\theta}_k^s\hat{\theta}_k^s + \hat{\phi}_k^s\hat{\phi}_k^s$, we can express the radiation pattern in (39) as

$$(\overline{\mathbf{I}}-\hat{k}_s\hat{k}_s)\cdot\hat{\beta}(\mathbf{x}'_{ij}) = \hat{\theta}_k^s[\hat{\theta}_k^s\cdot\hat{\beta}(\mathbf{x}'_{ij})] + \hat{\phi}_k^s[\hat{\phi}_k^s\cdot\hat{\beta}(\mathbf{x}'_{ij})]. \tag{40}$$

From the above expression, we can see that only two components or two radiation patterns need to be kept for each unknown component at a source point in the matrix equation.

For the compressional wave part, the related kernel can be written as

$$\overline{\mathbf{G}}_c(\mathbf{x}_{pq},\mathbf{x}'_{ij}) = -\frac{1}{\gamma}\frac{\nabla\nabla}{k_c^2}g_c(\mathbf{x}_{pq},\mathbf{x}'_{ij}) = \frac{1}{\gamma}\int d^2\hat{k}_c e^{i\mathbf{k}_c\cdot(\mathbf{r}_{bm}-\mathbf{r}_{am'})}\alpha_{mm'}(\mathbf{k}_c,\mathbf{r}_{mm'})\hat{k}_c\hat{k}_c \tag{41}$$

and the terms in the square brackets in the matrix equation (37) are then

$$\hat{\alpha}(\mathbf{x}_{pq})\cdot\overline{\mathbf{G}}_c(\mathbf{x}_{pq},\mathbf{x}'_{ij})\cdot\hat{\beta}(\mathbf{x}'_{ij}) = \hat{\alpha}(\mathbf{x}_{pq})\cdot\frac{1}{\gamma}\int d^2\hat{k}_c e^{i\mathbf{k}_c\cdot\mathbf{r}_{bm}}\alpha_{mm'}(\mathbf{k}_c,\mathbf{r}_{mm'})\cdot\left\{e^{-i\mathbf{k}_c\cdot\mathbf{r}_{am'}}\cdot\hat{k}_c[\hat{k}_c\cdot\hat{\beta}(\mathbf{x}'_{ij})]\right\}. \tag{42}$$

It can be seen that only one radiation pattern needs to be kept for each unknown component in this case. Therefore, there are three radiation patterns (the shear wave part has $\hat{\theta}_k$ and $\hat{\phi}_k$ components and compressional wave part has k component) in total for each unknown component. Since we have three unknown components for each unknown vector, we have nine radiation patterns in total now and a half number of radiation patterns is reduced if compared with the original scheme. The key step in the pattern reduction scheme is the use of spherical coordinates in the $\hat{k}$ space where $\hat{k}$ corresponds to $\hat{r}$ in a spherical coordinate system. The radiation patterns are the $\hat{\theta}_k$, $\hat{\phi}_k$ and $\hat{k}$ components in this space. When we make a translation in $\hat{r}$ space, these patterns remain invariant because they belong to $\hat{k}$ space.

6. Numerical examples

We demonstrate the proposed MLFMA by solving several relatively large problems with spherical geometries and comparing the solutions with the corresponding analytical solutions. In the implementation, the object geometries are discretized into triangular meshes and an one-point quadrature rule based Nyström method is used. This is because the cost will dramatically increase if we use a higher-order quadrature rule (the higher-order quadrature rule based Nyström method is usually used for small problems). Also, the Nyström method with the one-point quadrature rule is equivalent to the BEM.

We first consider the scattering by a fixed rigid sphere with a normalized radius of $k_c a = 16.0$, where k_c is the wave number of the incident wave and a is the radius of the sphere. The surrounding medium has Poisson's ratio $v = 0.1$ and mass density $\rho = 1.0$. The incident wave is a time-harmonic plane compressional wave with a unit circular frequency ($\omega = 1.0$). Fig. 2 illustrates the solution for the total traction field along the principal cut ($\phi = 0^\circ$ and $\theta = 0$—180°) at the sphere surface and the solution is close to the analytical counterpart. The used number of levels is $L = 5$ and the number of unknowns reaches $K = 305,280$. The consumed CPU time is $T = 219,167$ seconds and the memory usage is $M = 12$ GB. Note that although the same number of levels is used for different trees here, the definition for well-separation groups and near terms is different in different trees due to the difference of the wave numbers and they cannot share the same tree. We also use the pattern reduction scheme to calculate the scattered displacement field along the principal cut at the $r = 5a$

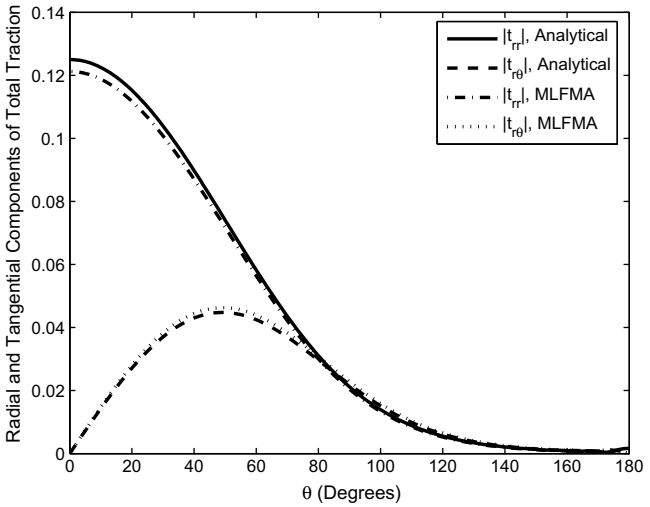

Fig. 2. Radial and tangential (elevated) components of total traction field along the principal cut at the surface of a rigid sphere, $k_c a = 16.0$.

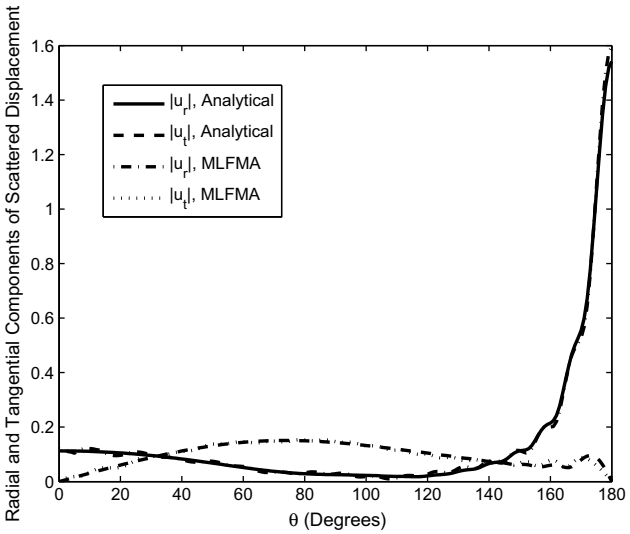

Fig. 3. Radial and tangential (elevated) components of scattered displacement field along the principal cut at the $r = 5a$ surface, $k_c a = 20.0$.

observation surface and Fig. 3 shows the solution with a comparison to the analytical counterpart. The computational conditions are the same as before except that $k_c a = 20.0$, $K = 317,196$ and $T = 182,347$ now. The proposed MLFMA can of course be applied to arbitrary 3D geometries. Fig. 4 illustrates the scattering solution by a rigid cube and no exact solutions can be used to compare with. The computational conditions are the same as those in the first case except that $K = 343,224$, $T = 230,672$ seconds, and the side length of the cube is $2a$ with $k_c a = 20.0$ now.

We then consider the scattering by a traction-free spherical cavity embedded in an elastic medium. The cavity also has a normalized radius of $k_c a = 16.0$ and the surrounding medium is characterized by Poisson's ratio $v = 0.1$, Young's modulus $E = 2/3$ and mass density $\rho = 1.0$. The incident wave is the same as that for the rigid sphere. Fig. 5 plots the solution for the scattered displacement field along the principal cut at the $r = 5a$ observation surface. The number of levels and number of unknowns are the same as those for the rigid sphere. The consumed CPU time is $T = 245,986$ seconds and the memory usage is $M = 12$ GB.

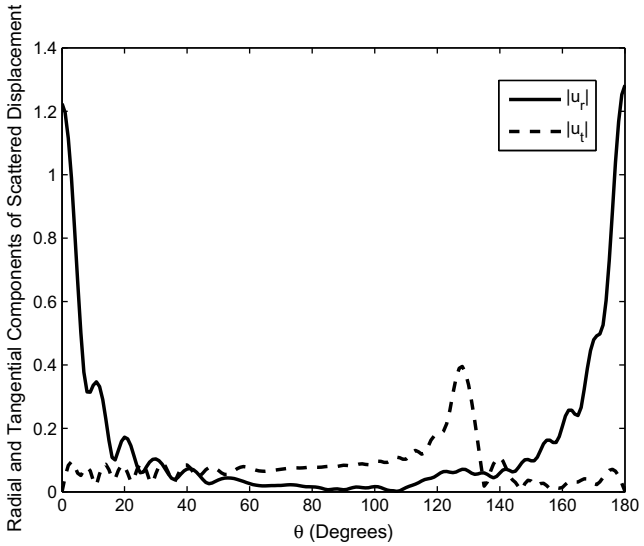

Fig. 4. Radial and tangential (elevated) components of scattered displacement field along the principal cut at the $r = 10a$ surface for a rigid cube with a side length of $2a$.

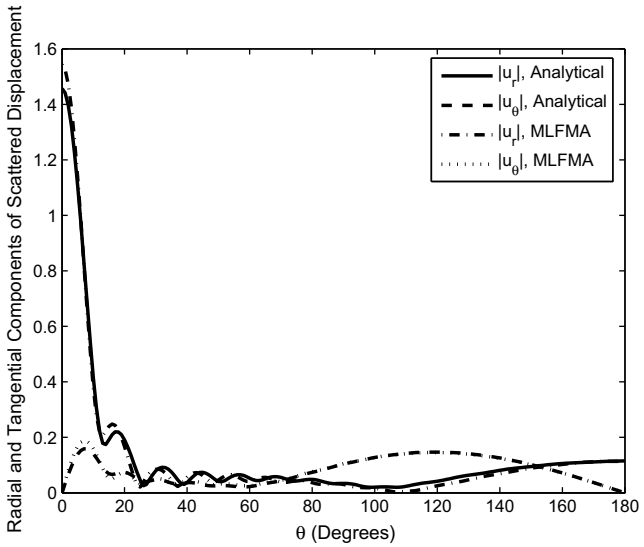

Fig. 5. Radial and tangential (elevated) components of scattered displacement field by a spherical cavity along the principal cut at the $r = 5a$ surface, $k_c a = 16.0$.

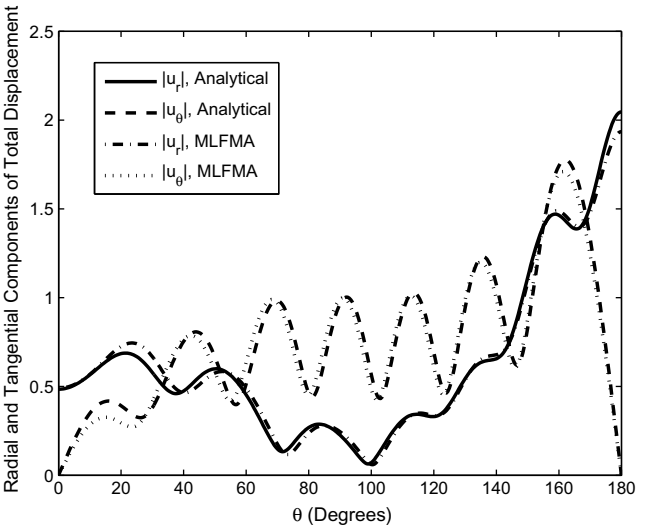

Fig. 6. Radial and tangential (elevated) components of total displacement field along the principal cut at the surface of an elastic sphere, $k_c a = 8.0$.

We finally consider the generalized case, i.e. both the object and surrounding media are elastic. We select $\lambda_1 = 0.1$, $\mu_1 = 0.4$ and $\rho_1 = 1.0$ for the surrounding medium, and $\lambda_2 = 0.2$, $\mu_2 = 0.5$ and $\rho_2 = 2.0$ for the elastic spherical object with a normalized radius of $k_c a = 8.0$. The incident wave is also the same as before. Fig. 6 shows the solution for the total displacement field along the principal cut at the sphere surface. The number of levels is $L = 4$ and the number of unknowns is $K = 237,600$. This problem is relatively small because there are four FMA trees in this case and the computational cost is much higher than those for rigid sphere and cavity scattering. The consumed CPU time and memory usage in this case are $T = 201,129$ seconds and $M = 12$ GB, respectively. From these figures, we can see that the MLFMA solutions are in good agreement with corresponding analytical solutions which can be found in [33].

7. Conclusion

We develop MLFMA for solving elastic wave scattering by large 3D objects. Since the governing BIE includes multiple wave numbers, a multiple-tree structure is used in the implementation of MLFMA. However, the multiple-tree frame will result in a nonuniform definition for well-separated groups and the cancellation of the strongest singularities in the series representation of kernels for near terms may be destroyed due to the disagreement of near-patch definition. We overcome this drawback by searching common near patches in different trees and reformulating the expressions of the near terms so that the cancellation of the strongest singularities is kept and the resulting singular integrals can be handled conveniently. Numerical examples have been used to demonstrate the feasibility of the proposed implementing scheme for the algorithm and fast solutions for the problems with 0.3–0.4 millions of unknowns have been achieved on a Dell Precision 690 workstation with two dual-core 3.0 GHz processors and 16 GB RAM but using a single core.

Acknowledgment

This work was supported by the Construction Engineering Research Laboratory (CERL), U.S. Army under Grant W9132T-06-2-0006.

References

[1] V. Rokhlin, Rapid solution of integral equations of classical potential theory, J. Comp. Phys. 60 (1985) 187–207.
[2] L. Greengard, The Rapid Evaluation of Potential Fields in Particle Systems, MIT Press, Cambridge, 1987.
[3] L. Greengard, V. Rokhlin, A fast algorithm for particle simulations, J. Comp. Phys. 73 (1987) 325–348.
[4] J. Carrier, L. Greengard, V. Rokhlin, A fast adaptive multipole algorithm for particle simulations, SIAM J. Sci. Comput. 9 (1988) 669–686.
[5] C.C. Lu, W.C. Chew, A multilevel algorithm for solving a boundary integral equation of wave scattering, Microw. Opt. Technol. Lett. 7 (1994) 466–470.
[6] J.M. Song, W.C. Chew, Multilevel fast-multipole algorithm for solving combined field integral equations of electromagnetic scattering, Microw. Opt. Technol. Lett. 10 (1995) 14–19.
[7] B. Dembart, E. Yip, A 3D fast multipole method for electromagnetics with multiple levels, in: Proc. 11th Ann. Rev. Prog. Appl. Comput. Electromagn., vol. 1, 1995, pp. 618–621.
[8] R. Coifman, V. Rokhlin, S. Wandzura, The fast multipole method for the wave equation: a pedestrian prescription, IEEE Antennas Propagat. Mag. 35 (1993) 7–12.
[9] M.F. Gyure, M.A. Stalzer, A prescription for the multilevel Helmholtz FMM, IEEE Comput. Sci. Eng. 5 (1998) 39–47.
[10] E. Darve, The fast multipole method: Numerical implementation, J. Comp. Phys. 160 (2000) 195–240.
[11] W.C. Chew, J.M. Jin, E. Michielssen, J.M. Song, Fast and Efficient Algorithms in Computational Electromagnetics, Artech House, Boston, 2001.

[12] J. Board, K. Schulten, The fast multipole algorithm, IEEE Comput. Sci. Eng. 2 (2000) 76–79.
[13] N. Nishimura, Fast multipole accelerated boundary integral equation methods, ASME Trans. Appl. Mech. Rev. 55 (2002) 299–324.
[14] J.M. Song, W.C. Chew, The fast Illinois solver code: requirements and scaling properties, IEEE Comput. Sci. Eng. 5 (1998) 19–23.
[15] J.M. Song, W.C. Chew, Large scale computations using FISC, IEEE Antennas Propagat. Int. Symp. 4 (2000) 1856–1859.
[16] S. Velamparambil, W.C. Chew, J.M. Song, 10 million unknowns: Is it that big?, IEEE Antennas Propagat Mag. 45 (2003) 43–58.
[17] M.L. Hastriter, A study of MLFMA for large scale scattering problems, Ph.D. Dissertation, ECE Dept. Univ. Illinois, Urbana, 2003.
[18] L. Gürel, Ö. Ergül, Fast and accurate solutions of extremely large integral-equation problems discretized with tens of millions of unknowns, Electron. Lett. 43 (2007) 499–500.
[19] Ö. Ergül, L. Gürel, Efficient parallelization of the multilevel fast multipole algorithm for the solution of large-scale scattering problems, IEEE Trans. Antennas Propagat. 56 (2008) 2335–2345.
[20] Y.H. Chen, W.C. Chew, Fast multipole method as an efficient solver for 2D elastic wave surface integral equations, Comput. Mech. 20 (1997) 495–506.
[21] T. Fukui, K. Inoue, Fast multipole boundary element method in 2D elastodynamics, J. Appl. Mech. JSCE 1 (1998) 373–380 (in Japanese).
[22] H. Fujiwara, The fast multipole method for integral equations of seismic scattering problems, Geophys. J. Int. 133 (1998) 773–782.
[23] T. Takahashi, N. Nishimura, S. Kobayashi, Fast boundary integral equation method for elastodynamic problems in 2D in time domain, Trans. JSMS (A) 67 (2001) 1409–1416 (in Japanese).
[24] K. Yoshida, N. Nishimura, S. Kobayashi, Analysis of three-dimensional scattering of elastic waves by crack with fast multipole boundary integral equation method, J. Appl. Mech. JSCE 3 (2000) 143–150 (in Japanese).
[25] H. Fujiwara, The fast multipole method for solving integral equations of three-dimensional topography and basin problems, Geophys. J. Int. 140 (2000) 198–210.
[26] T. Takahashi, N. Nishimura, S. Kobayashi, A fast BIEM for three-dimensional elastodynamics in time domain, Eng. Anal. Bound. Elem. 27 (2003) 491–506.
[27] Y. Otani, N. Nishimura, A fast multipole boundary integral equation method for period boundary value problems in three-dimensional elastostatics and its application to homogenisation, Int. J. Multiscale Comput. Eng. 4 (2006) 487–500.
[28] T. Saitoh, S. Hirose, T. Fukui, Application of fast multipole boundary element method to multiple scattering analysis of acoustic and elastic waves, AIP Conf. Proc. 894 (2007) 79–86.
[29] Y. Otani, N. Nishimura, An FMM for periodic boundary value problems for cracks for Helmhotz' equation in 2D, Int. J. Numer. Meth. Eng. 73 (2008) 381–406.
[30] M.S. Tong, W.C. Chew, Nyström method for elastic wave scattering by three-dimensional obstacles, J. Comput. Phys. 226 (2007) 1845–1858.
[31] Y.H. Pao, V. Varatharajulu, Huygens' principle, radiation conditions, and integral formulas for the scattering of elastic waves, J. Acoust. Soc. Amer. 59 (1976) 1361–1371.
[32] F.J. Rizzo, D.J. Shippy, M. Rezayat, A boundary integral equation method for radiation and scattering of elastic waves in three dimensions, Int. J. Numer. Methods Eng. 21 (1985) 115–129.
[33] Y.-H. Pao, C.C. Mow, Scattering of plane compressional waves by a spherical obstacle, J. Appl. Phys. 34 (1963) 493–499.